19

Modelling Groundwater Contamination Above High-Level Nuclear-Waste Repositories in Salt, Granitoid and Clay

Michal O. Schwartz
MathGeol
Germany

1. Introduction

Modelling the groundwater contamination in the aquifer above a repository for high-level nuclear waste is a complex task. The usual procedure is based on modelling the transport of radionuclides in one or two dimensions only (NAGRA, 2002; Kosakowski, 2004; Keesmann et al., 2006; SKB, 2006; Nykyri et al., 2008). However, modern computing techniques allow to perform simulations in three dimensions, which are a more realistic representation of the geosphere or far field. This is shown for candidate repositories in salt (Gorleben, Germany) and granitoid (Olkiluoto, Finland). To date, is not possible to conduct similar three-dimensional simulations for a repository in clay because the necessary input data are not available. Nevertheless, it can be shown that the results obtained from the simulations with a granitoid-hosted repository are useful for evaluating the performance of a clay-hosted repository. The objective of this comparative study is to provide tools that facilitate the identification of disposal sites and enhance the transparency of decision-making processes.

2. Computer codes for flow-transport models

The generation of a gas phase is an important issue for a repository in salt. Therefore, both one-phase (liquid only) and two-phase (liquid and gas) simulations are performed for the salt-hosted Gorleben repository. The two-phase simulations are performed with the TOUGHREACT code (Xu et al., 2005). This is a numerical simulation program that calculates chemically reactive non-isothermal flows of multi-phase fluids and geochemical transport in porous and fractured media. The program was developed by introducing reactive chemistry into the multi-phase flow code TOUGH2 (Pruess et al., 1999). The code performs a fully coupled simultaneous solution of mass and energy balance for multicomponent fluids, combined with a multiphase extension of Darcy's Law and Fickian diffusion. The program consists of a number of functional units with flexible and transparent interfaces. The governing equations are discretised using integral finite difference for space and fully implicit first-order finite difference in time. The resulting non-linear algebraic equations are solved by Newton-Raphson iteration. The simulations are performed with the ECO2 module, which treats the aqueous phase as a mixture of water and salt. The dependence of density, viscosity, enthalpy and vapour pressure on salt

concentration is taken into account, as well as the effects of salinity on gas solubility in the liquid phase and related heat of solution.

The one-phase scenario for Gorleben is calculated with TOUGH2-MP (Zhang et al., 2008), the parallel version of the TOUGH2 code. The EOS7R module is used, which calculates the transport of a parent radionuclide and a daughter radionuclide. The aqueous phase is treated as a mixture of water and brine.

For a granitoid-hosted repository, the potential gas release is negligibly small. Therefore, only a one-phase scenario is calculated for the Olkiluoto repository. The TOUGHREACT code with the ECO2 module is used for these simulations.

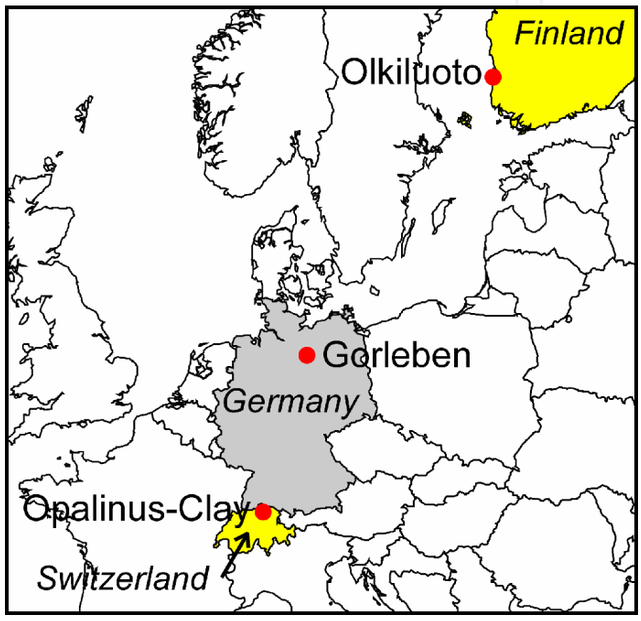

Fig. 1. Location of the candidate repositories Gorleben (Germany), Olkiluoto (Finland) and Opalinus Clay (Switzerland)

3. The salt-hosted repository at Gorleben

3.1 Repository layout

The repository (Figs. 1 and 2) will accommodate 5,440 waste containers with a total of 8,550 t U of burnt fuel (Keesmann et al., 2005). The waste containers, which are made of Mn-Ni steel, have a length of 5.5 m and a diameter of 1.6 m (Javeri, 2006). They will be emplaced in horizontal disposal drifts, which will be connected to two or more shafts by a system of access drifts. The envisaged disposal depth is about 800 m. There are 260-280 m Quaternary-Tertiary siliciclastic sediments above the present mine workings within the Zechstein salt dome.

3.2 Near field

The near field is the hydrochemical regime of the backfilled underground workings in the salt dome and the far field is hydrochemical regime of the caprock and cover sediments. The

far-field simulations use the near-field releases as input. To date, only two near-field scenarios have been published. The first considers a single-phase case with liquid-phase transport only. The second considers a two-phase case with both liquid-phase and gas-phase transport.

The near-field release of the single-phase scenario (Fig. 3; Keesmann et al., 2005) is the latest update of the Early-Intrusion-Case of Storck et al. (1988). About 2,000 m^3 of brine is assumed to intrude into the repository and dissolve the waste up to the solubility limits shown in Table 1. The brine is squeezed out of the repository due to the convergence of the elastically deforming rock salt. The exit point of the contaminated brine is the contact between Quaternary sediments and the Main Anhydrite (Hauptanhydrit) of the Zechstein salt dome at the borehole location GoHy3020 (Fig. 2) on the -250-m level.

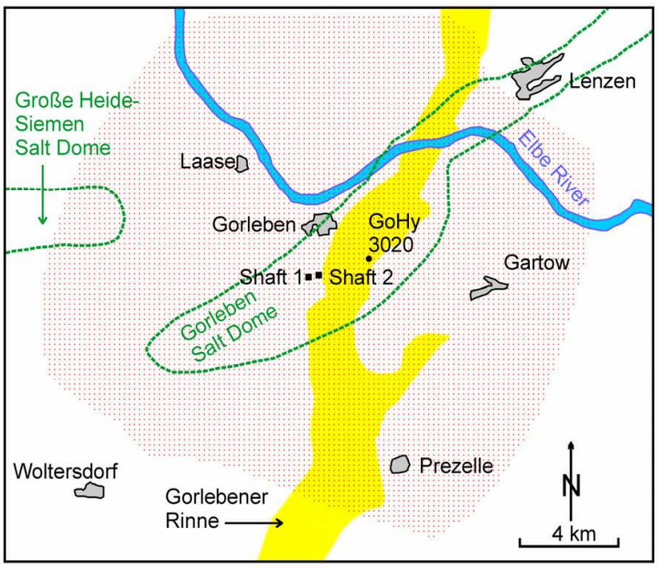

Fig. 2. Map of the Gorleben area with model mesh

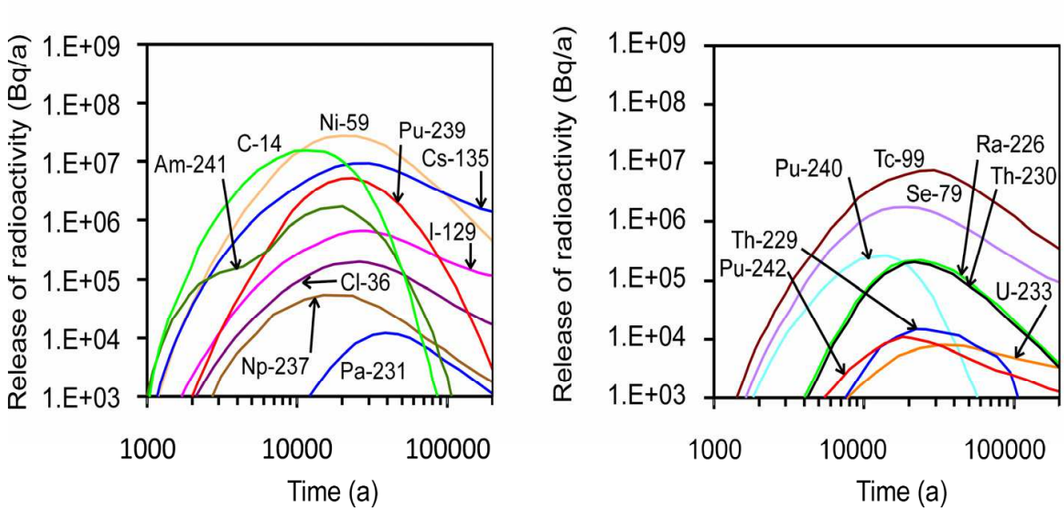

Fig. 3. Gorleben model. Near-field release of radionuclides (Bq/a) for the one-phase scenario

The two-phase scenario for the release of C-14 in the presence of a gas phase is based on a case described by Javeri (2006). Brine squeezed out from a 1,000 m^3 brine pocket intrudes a backfilled disposal drift during 2,000 years following the closure of the repository. The disposal drift hosts 33 waste containers. At low oxygen fugacities, the container wall is subjected to corrosion dominated by the reaction

$$3Fe + 4H_2O = Fe_3O_4 + 4H_2. \quad (1)$$

The corrosion process releases hydrogen gas at a rate that increases from zero to 3.84 kg/a in the period from year zero to year 100 and decreases from 3.84 kg/a to zero in the period from year 20,000 to year 40,000. The hydrogen gas leaves the repository via the backfilled shaft according to the release rates shown in Figure 4.

Solubility (mol/L)					
	One-phase scenario	**Two-phase scenario**		**One-phase scenario**	**Two-phase scenario**
Am	$1.0x10^{-5}$	-	Pa	$1.0x10^{-6}$	-
C	$1.0x10^{-2}$	unlimited	Pu	$1.0x10^{-6}$	-
Cl	unlimited	-	Ra	$1.0x10^{-6}$	-
Cs	unlimited	-	Se	$1.0x10^{-4}$	-
I	unlimited	-	Tc	$1.0x10^{-4}$	-
Ni	$1.0x10^{-4}$	-	Th	$1.0x10^{-6}$	-
Np	$1.0x10^{-5}$	-	U	$1.0x10^{-4}$	-

Table 1. Gorleben model. Liquid-phase solubility in the near field

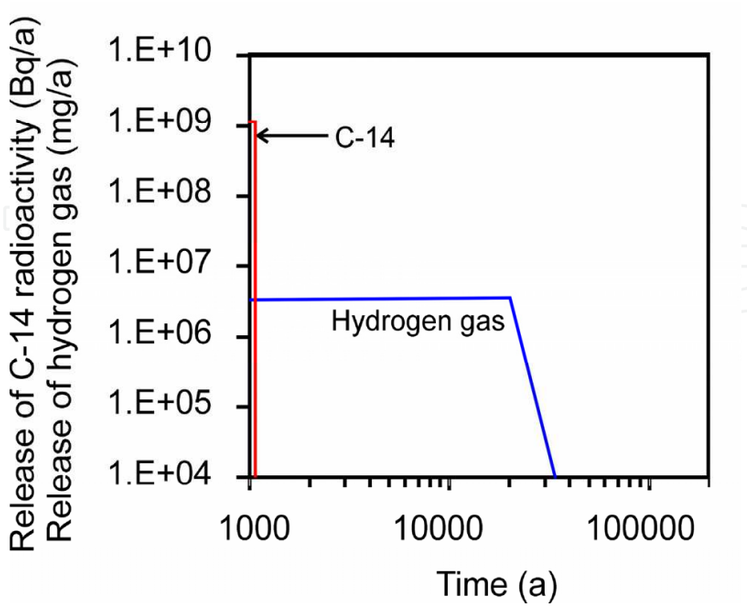

Fig. 4. Gorleben model. Near-field release of hydrogen gas (mg/a) and C-14 (Bq/a) for the two-phase scenario

Fig. 5. Gorleben model. Block diagram. Vertical exaggeration ratio 12:1

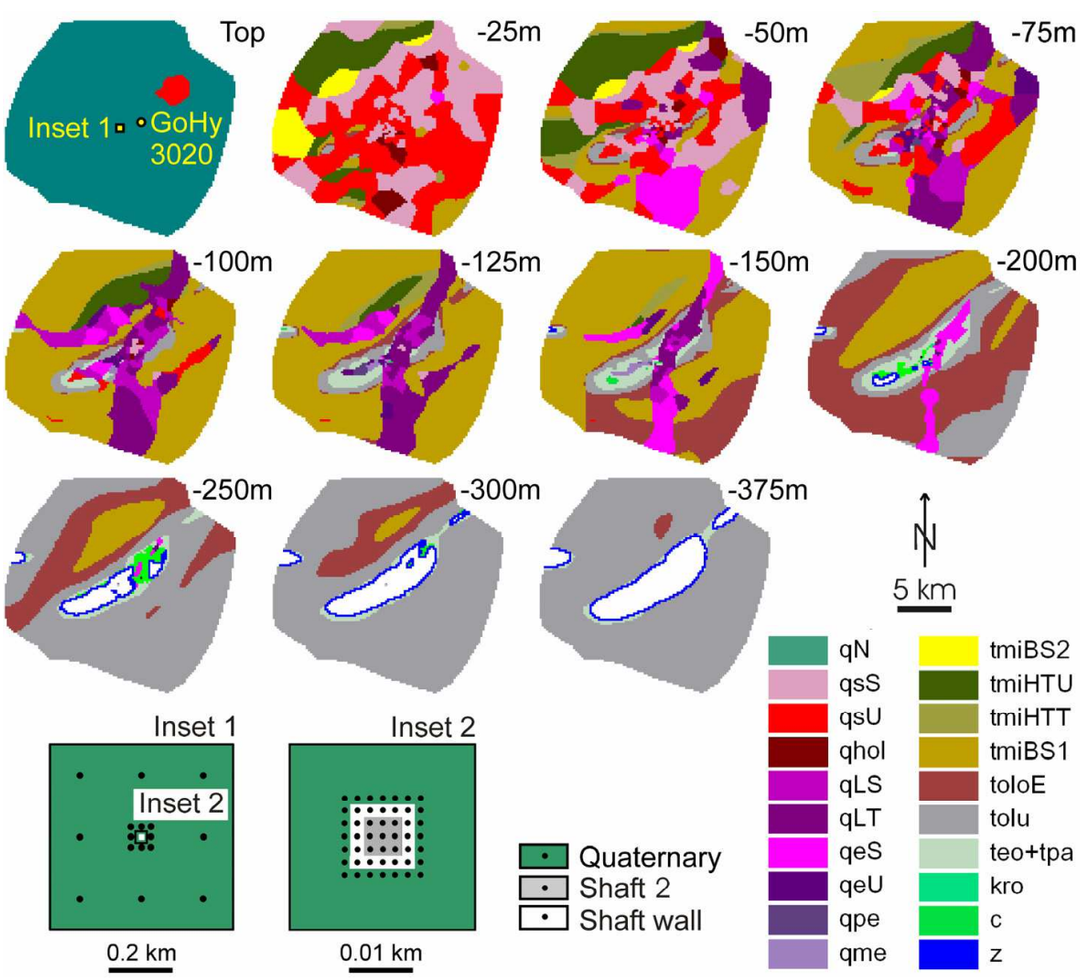

Fig. 6. Gorleben model. Hydrostratigraphic units (Table 3) of the top, -25 m, -50 m, -75 m, -100 m, -125 m, -150 m, -200 m, -250 m, -300 m and -375 m layer. The location of the borehole GoHy3020 and the structure of the mesh in the area surrounding Shaft 2 (Insets 1 and 2) are also shown

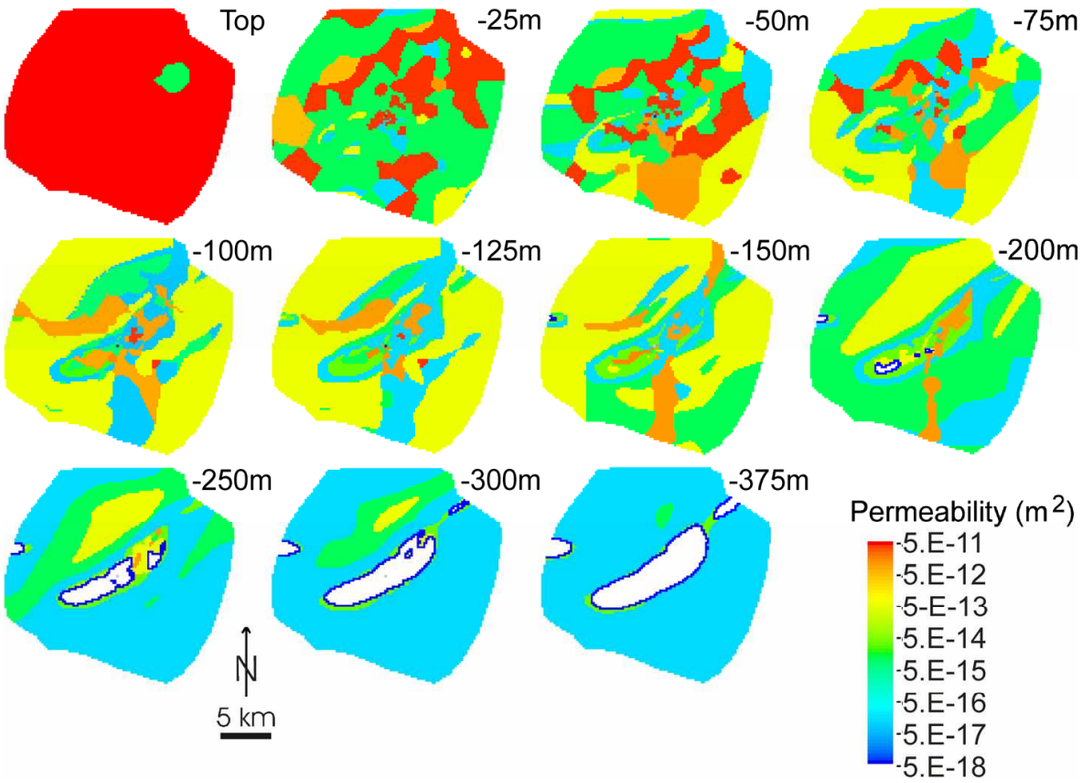

Fig. 7. Gorleben model. Permeability (m^2) of the top, -25 m, -50 m, -75 m, -100 m, -125 m, -150 m, -200 m, -250 m, -300 m and -375 m layer

Together with hydrogen, C-14 species are released. The average waste canister contains C-14 with an activity of 3 x 10^{10} Bq (Keesmann et al., 2005). A fraction of 15 % is available for rapid release upon failure of the canister. This is assumed to result in a release of 13 % of the initial C-14 inventory out of the repository during a 100-year period starting in the year 1,000 after the closure of the repository. The corresponding release from the total of the 33 waste containers is 1.3 x 10^9 Bq/a. C-14 is the only radionuclide considered in the two-phase scenario because it is the only long-lived radionuclide that strongly partitions into the gas phase.

TOUGHREACT allows for injection of a single non-condensable gas, which is hydrogen in the case of the present study. Other gaseous species are introduced as secondary species via the corresponding primary liquid species according to a dissociation reaction such as

$$HCO_3^- + H^+ = CO_{2(gas)} + H_2O. \quad (2)$$

The primary species are HCO_3^-, H^+ and $O_{2(aq)}$. The secondary species are $CO_{2(gas)}$, $CH_{4(gas)}$, $CH_{4(aq)}$, $CO_{2(aq)}$ and CO_3^{-2}. The initial and boundary solutions have a H^+ activity of 10^{-7} and an $O_{2(aq)}$ activity of 10^{-67}. The source for the two-phase model is the near-field release shown in Figure 4. Hydrogen gas is injected into the primary central cell of shaft 2 on the -237.5-m level whereas a boundary solution with HCO_3^- is injected from a secondary boundary cell that is connected to this primary cell.

General properties					
Model length/width/height (m)		22,400/21,000/400			
Model temperature (°C)		25			
Simulation period (a)		200,000			
Rock density (kg/dm³)		2.5			
Saturated hydraulic properties (Table 3)					
Permeability (m²)		$5x10^{-11}$-$1x10^{-18}$			
Porosity (-)		0.03-0.3			
Unsaturated hydraulic properties					
Residual liquid saturation		0.			
Residual gas saturation		0.			
Van Genuchten parameter α (Pa)		$4.46x10^{4}$			
Van Genuchten parameter *m* (-)		0.21			
Distribution coefficients (dm³/kg)					
	One-phase scenario				**Two-phase scenario**
	Low-salinity water (<10 g/L salt)		**High-salinity water (≥10 g/L salt)**		**Low/high-salinity water**
	Sand	Silt/clay	Sand	Silt/clay	Sand/silt/clay
Am	300	20,000	3,000	20,000	-
C	0.2	2	0.2	2	0.
Cl	0.1	0.1	0.1	0.1	-
Cs	70	400	2	70	-
I	2	2	0.1	2	-
Ni	20	300	6	90	-
Np	10	300	10	300	-
Pa	600	6,000	600	6,000	-
Pu	100	3,000	100	3,000	-
Ra	40	300	2	40	-
Se	1	1	1	1	-
Tc	1	6	1	1	-
Th	200	2,000	200	200	-
U	2	80	0.6	20	-
Aqueous phase diffusivity (m²/s)					
Salt	$1.0x10^{-7}$				
Hydrogen	$1.0x10^{-9}$				
All radionuclides	$1.0x10^{-9}$				

Table 2. Set-up of the Gorleben far-field model

Quaternary			
Symbol	**Rock**	**Permeability (m^2)**	**Porosity (-)**
qN	Holocene, Weichsel glacial (sand)	$5x10^{-11}$	0.3
qsS	Saale glacial (sand)	$4x10^{-11}$	0.3
qsU	Saale glacial (silt, clay, drift marl)	$1x10^{-14}$	0.15
qhol	Holstein interglacial (silt, clay)	$1x10^{-16}$	0.03
qLS	Elster glacial/Lauenburger-Ton-Komplex (sand)	$1x10^{-11}$	0.3
qLT	Elster glacial/Lauenburger-Ton-Komplex (clay, silt)	$1x10^{-16}$	0.03
qeS	Elster glacial [excluding Lauenburger-Ton-Komplex] (sand)	$1x10^{-11}$	0.3
qeU	Elster glacial [excluding Lauenburger-Ton-Komplex] (silt, drift marl)	$1x10^{-14}$	0.15
qpe	Bavel-Cromer-Komplex (silt)	$1x10^{-14}$	0.15
qme	Menap glacial (sand)	$1.5x10^{-11}$	0.3
Tertiary/Cretaceous/Zechstein			
Symbol	**Rock**	**Permeability (m^2)**	**Porosity (-)**
tmiBS2	Lower Miocene/Obere Braunkohlensande (sand)	$5x10^{-12}$	0.3
tmiHTU	Lower Miocene/Hamburger-Ton-Komplex (silt, clay, sand)	$1x10^{-14}$	0.15
tmiHTT	Lower Miocene/Hamburger-Ton-Komplex (clay, silt)	$1x10^{-16}$	0.03
tmiBS1	Lower Miocene/Untere Braunkohlensande [includ. Neochat] (sand, silt)	$5x10^{-13}$	0.3
toloE	Upper Oligocene/Eochat (clay, silt)	$1x10^{-14}$	0.15
tolu	Lower Oligocene/Rupelton (clay, silt)	$1x10^{-16}$	0.03
teo+tpa	Eocene, Paleocene (clay, silt, sand)	$3x10^{-14}$	0.15
kro	Cretaceous (limestone, marlstone, sand)	$1x10^{-14}$	0.15
c	Caprock (former Zechstein salt)	$5x10^{-13}$	0.3
z	Zechstein salt	$1x10^{-18}$	0.1
Structural material			
	Permeability (m^2)	**Porosity (-)**	
Backfill of Shaft 2	$3x10^{-13}$ - $3x10^{-12}$	0.3	
Wall of Shaft 2	$1x10^{-16}$	0.1	

Table 3. Saturated hydraulic properties of rocks and structural material of the Gorleben far-field model

3.3 Geometry of the far-field model and initialisation

The irregular mesh has 290,435 elements and measures 22,400 m x 21,000 m x 400 m (Figs. 5-7; Table 2). Three sets of nodal distances in the x and y direction are used. The backfilled shaft 2, which measures 6 x 6 m horizontally, and the area immediately surrounding shaft 2 (shaft wall and bedrock) have horizontal nodal distances of 2 m. An intermediate zone (only bedrock) has horizontal nodal distances of 20 m. The remaining part of the primary mesh (only bedrock) has nodal distances of 200 m.

The top layer has nodal z values representing the head (between 12.7 m and 22.1 m altitude; Fig. 8). The second layer has nodes located 0.1 m vertically below those of the top layer. The vertical nodal distance between the following 32 layers is 12.5 m. The top layer, which serves to maintain constant pressure and salinity, exclusively consists of infinite-volume boundary elements (10^{45} m^3). Other boundary cells are the rock-salt cells and the bottom-layer cells of the -375-m level. They have a volume of 10^{14} m^3. This volume is large enough for maintaining nearly constant salinity throughout the simulation period but is simultaneously flexible enough to account for pressure adjustments. The volume of the remaining cells is calculated according to their nodal positions. A secondary boundary cell is connected to the primary cell in the centre of shaft 2 at the top of the salt dome (-237.5-m level). The boundary cell is used for injecting HCO_3^- whereas the primary cell is used for injecting hydrogen gas.

The initialisation starts with a pressure of 10^5 Pa in all models cells. The infinite-volume elements of the top layer have zero salinity. The large-volume elements (10^{14} m^3) for the rock-salt unit and the bottom layer have an initial salinity of $X_{brine} = 1$ ($X_{salt} = 0.25$). Based on these boundary conditions, the diffusivity of brine is estimated in a trial-and-error procedure. Suitable vertical salinity gradients at the end of the 100,000-year initialisation period are obtained with a diffusivity 10^{-7} m^2/s (Fig. 9). These salinity gradients, which are close to the present-day values (Klinge et al., 2007), are maintained with insignificant variations throughout the following 7,000-year and 200,000-year simulation periods.

3.4 Hydrostratigraphy and hydraulic properties

The hydrostratigraphic information of 197 drill hole logs is transferred to the nearest model node at the corresponding z-position (Figs. 6 and 8; Ludwig et al., 1989; Beushausen & Ludwig, 1990; Ludwig et al., 1993; Klinge et al., 2001). Based on this information, the hydrostratigraphic units for the remaining nodes are assigned by interpolation and extrapolation.

The saturated hydraulic properties of the hydrostratigraphic units of the caprock and cover sediments (Table 3) are assigned according to Vogel (2005). This scheme is based on the geometric mean of empirical maximum and minimum values. No decision has been taken yet with respect to the saturated hydraulic properties of the backfill of shaft 2. Therefore, various permeability cases are calculated (base-case permeability of 1 x 10^{-12} ; sensitivity cases of 3 x 10^{-13}, 5 x 10^{-13}, 2 x 10^{-12} and 3 x 10^{-12} m^2). The porosity is 0.3 for all cases.

The unsaturated permeabilities are calculated with the relative-permeability function of Corey (1954; quoted by Brooks & Corey, 1964). The parameters for the capillary-pressure function of Van Genuchten (1980) are those of the Apache Leap tuff reported by Rasmussen (2001).

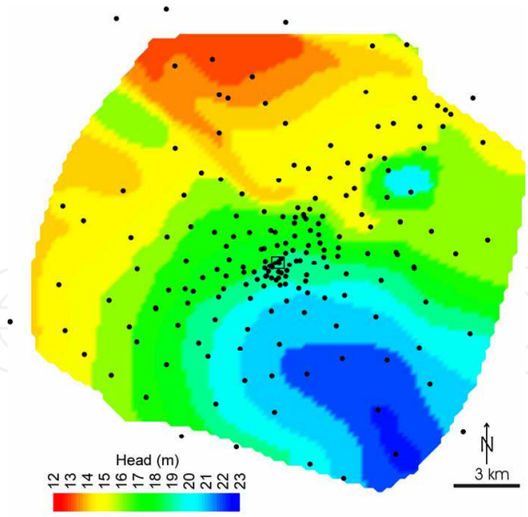

Fig. 8. Gorleben model. Head (m), location of Shaft 2 (open black square) and boreholes (solid black circles)

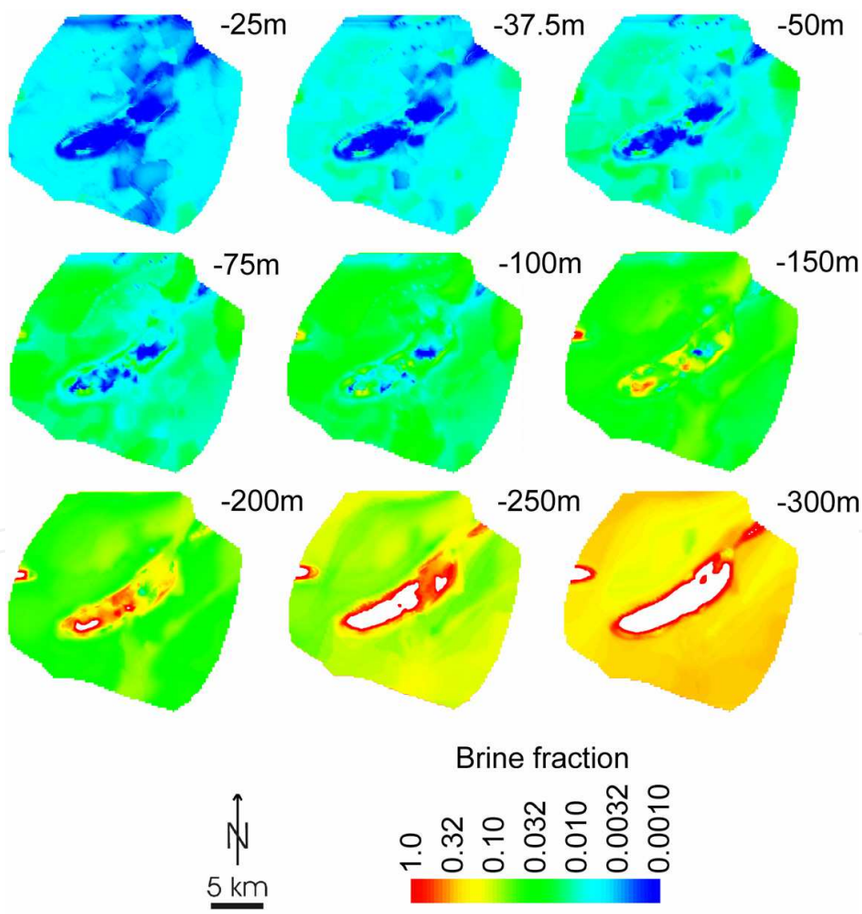

Fig. 9. Gorleben model. Salinity (brine fraction) of the -25 m, -37.5 m, -50 m, -75 m, -100 m, -150 m, -200 m, -250 m, and -300 m layer

	Inventory (Bq/t U)	Half-life (a)	Dose conversion factor (Sv/a:Bq/L)
Am-241 (parent of Np-237)	2.05×10^{14}	432	3.4×10^{-4}
C-14	1.89×10^{10}	5,700	5.9×10^{-5}
Cl-36	3.43×10^{8}	3.0×10^{5}	9.5×10^{-6}
Cs-135	2.18×10^{10}	2.0×10^{6}	3.7×10^{-6}
I-129	2.02×10^{9}	1.6×10^{7}	2.1×10^{-4}
Ni-59	6.02×10^{10}	7.5×10^{4}	5.4×10^{-8}
Np-237	1.34×10^{10}	2.1×10^{6}	7.5×10^{-4}
Pa-231	1.27×10^{6}	3.3×10^{4}	2.0×10^{-3}
Pu-239 (parent of U-235)	2.16×10^{13}	2.4×10^{4}	3.5×10^{-4}
Pu-240 (parent of U-236)	5.11×10^{13}	6.5×10^{3}	3.5×10^{-4}
Pu-242 (parent of U-238)	3.78×10^{11}	3.7×10^{5}	3.2×0^{-4}
Ra-226	1.06×10^{4}	1.6×10^{3}	1.8×10^{-4}
Se-79	1.75×10^{10}	1.1×10^{6}	6.1×10^{-7}
Tc-99	2.54×10^{11}	2.1×10^{5}	6.3×10^{-7}
Th-229	6.45×10^{3}	7.9×10^{3}	6.7×10^{-4}
Th-230 (parent of Ra-226)	3.92×10^{6}	7.5×10^{4}	1.1×10^{-4}
U-233	3.62×10^{6}	1.6×10^{5}	4.7×10^{-5}
U-235	4.97×10^{8}	7.0×10^{8}	4.5×10^{-5}
U-236	8.43×10^{9}	2.3×10^{7}	4.4×10^{-5}
U-238	1.22×10^{10}	4.5×10^{9}	4.2×10^{-5}

Table 4. Inventory of radionuclides in the candidate repository at Gorleben, half-life of radionuclides and dose conversion factor (DCF)

3.5 Sorption and diffusion

The distribution coefficients for the radionuclides in the one-phase scenario are taken from Suter et al. (1998). C-14 in the two-phase scenario is assumed to be non-sorbing under low oxygen fugacities compatible with the release of hydrogen gas. The aqueous phase diffusivity is 10^{-9} m²/s for all species (Keesmann et al., 2005).

3.6 Simulated far-field transport

The simulation period is from year 1,000 to year 200,000 for the single-phase scenario and from year 1,000 to year 8,000 for the two-phase scenario. The input for the one-phase simulations is the near-field release of 17 radionuclides, of which five are the parents for daughter radionuclides (Am-241, Pu-239, Pu-240, Pu-242 and Th-230; Fig. 3; Table 4). The biosphere is represented by the -37.5-m level, which approximately is the limit between fresh water and saline water (1 g/L salt or 0.0034 brine fraction). The radioactive plume reaches its highest vertical extent in the year 200,000 (end of the simulation period) and in the year 7,000 for the one-phase and two-phase scenario, respectively (Figs. 10 and 11).

The calculation of the radioactive dose is based on Dose Conversion Factors (DCFs; Table 4; Hirsekorn et al., 1991). The annual dose D_D (Sv/a) is calculated according to the equation

$$D_D = \sum X_i C_i \ \text{[Sv/a]}, \tag{3}$$

where X_i is the concentration (Bq/L) of the radionuclide i and C_i is the DCF (Sv/a:Bq/L) of the radionuclide i.

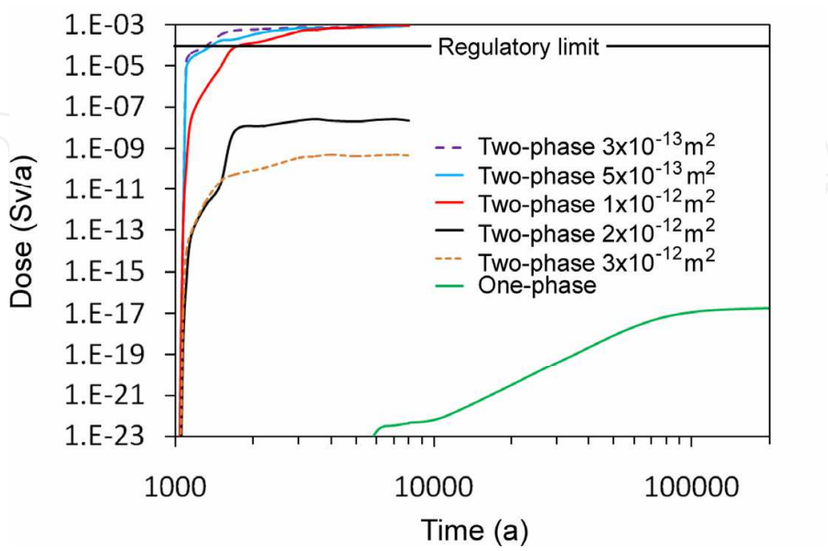

Fig. 10. Gorleben model. Peak values of the radioactive dose (Sv/a) on the -37.5 m level for the one-phase scenario and two-phase scenario (base case with a permeability of 1 x 10^{-12} m^2 for the backfill of Shaft 2 and sensitivity cases with a permeability of 3 x 10^{-13} m^2, 5 x 10^{-13} m^2, 2 x 10^{-12} m^2 and 3 x 10^{-12} m^2)

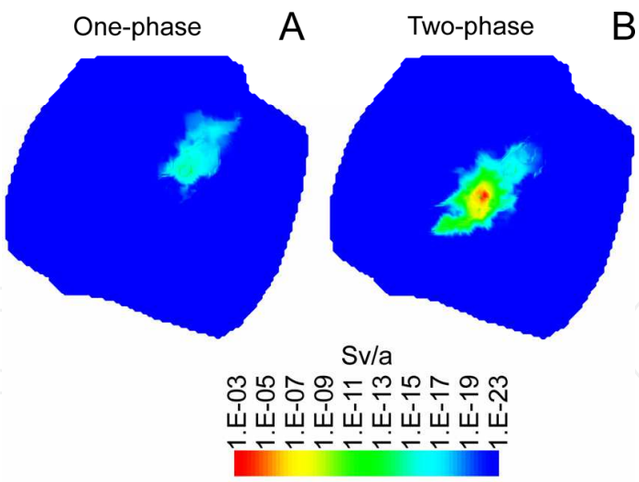

Fig. 11. Gorleben model. (A and B) Maps of the -37.5-m layer with radioactive dose (Sv/a) in the simulation year 200,000 for the one-phase scenario and year 7,000 for the base case of the two-phase scenario

For the single-phase scenario, the peak doses on the -37.5-m level is 1 x 10^{-17} Sv/a. For the two-phase scenario, the peak dose varies strongly depending on the assumptions for the permeability of the backfill of shaft 2. For the base-case permeability (1 x 10^{-12} m^2) and lower permeabilities, the peak dose is above the German regulatory limit of 1 x 10^{-4} Sv/a.

4. The granitoid-hosted repository at Olkiluoto

4.1 Repository layout

The planned repository is located in granitoid at 420 m depth at the island of Olkiluoto off the south-west coast of Finland (POSIVA, 2009). It can accommodate 3,000 containers with a total of 5,800 t U of burnt fuel (Löfman, 2005). According to the KBS-3V concept, the containers will be emplaced in vertical deposition holes driven from the floor of deposition tunnels, which are connected to a nearly horizontal system of access tunnels and transport tunnels. The containers that host the waste have a 5 cm thick corrosion-resistant copper shell around an inner deformation-resistant cast-iron canister; they are embedded in a 35 cm thick bentonite buffer. The horizontal dimensions of the repository are 1,600 m x 1,400 m.

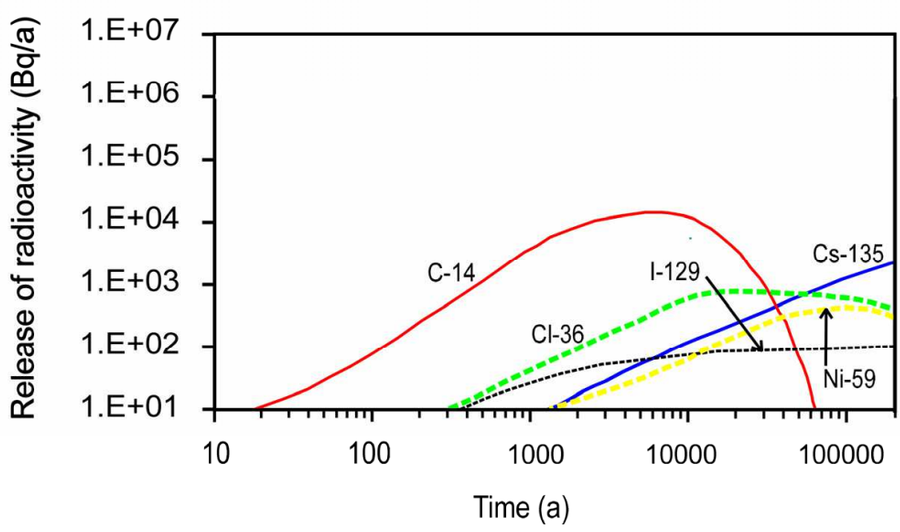

Fig. 12. Olkiluoto model. Near-field release of radionuclides (Bq/a)

4.2 Near-field

The near field is the hydrochemical regime of the underground workings and engineered barrier around the radioactive waste, consisting of the container wall and bentonite buffer. The reference failure mode for a defective canister and release of radioactivity from the near field to the undisturbed rock of the far field (geosphere) is the near-field base case (Nykyri et al., 2008). The canister is assumed to have a production defect with a diameter of 1 mm through which water enters into the canister causing dissolution of the fuel up to the solubility limits shown in Table 5. The near-field release of radionuclides (Fig. 12) is used as source for the contaminant injection cells in the far-field model.

As opposed to the easily corrodible steel canisters in the salt repository (see above), the copper shell of the canisters in the granitoid repository (KBS-3V concept) has an extraordinary chemical stability (Schwartz, 2008). Among the various candidate materials for waste packages, copper has unique oxidation characteristics. The conversion from native metal (Cu°) to metal oxide (Cu_2O) occurs in a mildly oxidising to mildly reducing environment (positive Eh for pH <7.7 at 25°C; Fig. 13) whereas the conversion of steel, titanium or nickel-chromium alloy already is possible under strongly reducing conditions,

i.e., below the stability field of liquid water. Native copper is present as natural occurrence in the Earth's crust. The largest deposits are located on the Keweenaw Peninsula of Michigan, where they have been mined to a depth of 2.2 km (Schwartz, 1996). These deposits formed one billion years ago at temperatures of 100-200°C. The mineralising fluids were slightly less reducing but had much higher copper concentrations than common present-day groundwater.

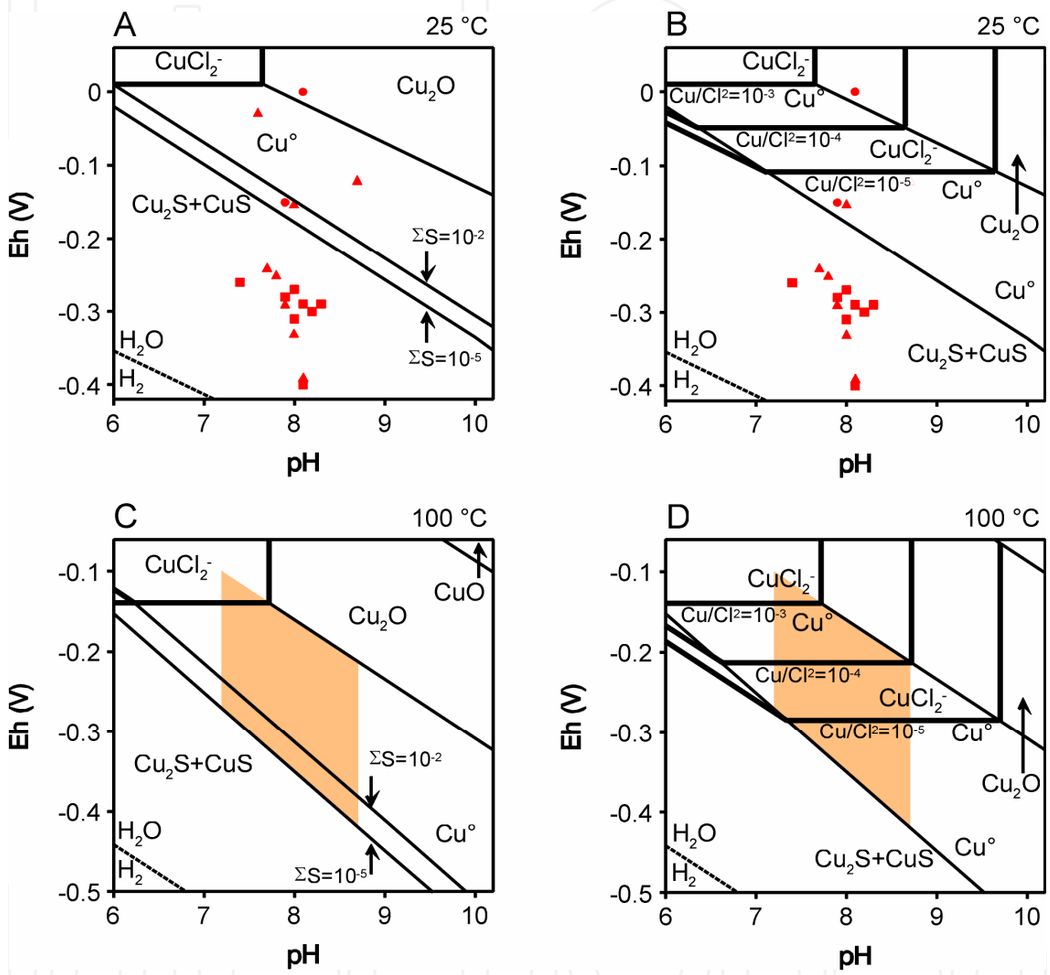

Fig. 13. Eh-pH diagrams for the system Cu-S-Cl-O-H at 25°C and 100°C for 0.1-0.3 mol/L Cl (Schwartz, 2008). Shaded area = Eh-pH range in which the Keweenaw native-copper deposits have formed (Schwartz, 1996). Point symbols = groundwater in crystalline rock of envisaged disposal sites in Sweden, Finland and Switzerland. (A and C) Diagrams for ΣS of 10^{-2} and 10^{-5}, and $\Sigma Cu/Cl^2 = 10^{-3}$. (B and D) Diagrams for $\Sigma S = 10^{-5}$ and $\Sigma Cu/Cl^2$ of 10^{-3}, 10^{-4} and 10^{-5}

Under the envisaged repository conditions, $CuCl_2^-$ is the dominant aqueous copper species. Accordingly, the thermodynamically relevant parameter is the $\Sigma Cu/Cl^2$ ratio, which refers to the sum of activities of all dissolved copper species divided by the Cl^- activity raised to the second power. Mine waters in the Keweenaw district have $\Sigma Cu/Cl^2$ ratios in the range from 10^{-4} to 10^{-5}. Similar conditions are achievable in the bentonite buffer around the copper

container if the bentonite contains artificial admixtures of fine-grained native copper. This is a technically feasible variant of the KBS-3V concept, which simulates the environment of a natural native-copper deposit. Thus thermodynamic equilibrium between container and fluid on the high Eh side of the native-copper stability field is implemented in the repository-container system as analogue to the natural counterparts.

The low-Eh and low-pH side of the native-copper stability field is the copper-sulphide phase boundary (CuS and CuS_2). The position of this boundary depends on the total activity of aqueous sulphur species (ΣS). The groundwater in the envisaged repositories in Finland, Sweden and Canada has ΣS in the range from $<10^{-5}$ to 10^{-2}. This implies conditions partly below the stability field of native copper, pH being in the range of 7-9 and Eh in the range from –0.03 to -0.4 V. Provided the bentonite contains no sulphur-bearing minerals, the corrosion of the copper container is constrained by the diffusion of aqueous sulphide from the granitoid aquifer through the bentonite to the container surface. This situation is quite different from corrosion of other package materials such as steel, titanium or nickel-chromium alloy, which all corrode by reaction with omnipresent water. It is not possible to control corrosion of these materials by a diffusion barrier around the container.

The reference buffer of the KBS-3V concept is the pyrite-bearing MX-80 bentonite (0.3 % sulphide sulphur). Another option is the Avonlea bentonite, which has no sulphides but a high content of gypsum (2 %). Neither the presence of pyrite (FeS_2) nor gypsum ($CaSO_4 \cdot 2H_2O$) is desirable because ΣS of the system should be as low as possible. The Czech EKOBENT bentonite (Prikryl & Woller, 2002), which has a total sulphur concentration of less than 0.05 % and does not contain sulphides, would be the better choice although it has not been tested as thoroughly as MX-80 or Avonlea. The original idea behind the use of a sulphide-bearing bentonite in the KBS-3V repository was to accelerate the transition from oxidising conditions (during the construction phase) towards a final anoxic regime. This scheme, however, has been called in question (SKI, 2006). There are alternatives such as the implementation of saturated conditions in the shortest possible time. This can be achieved by incremental flooding of those parts of the slightly inclined emplacement tunnels where waste packages are already in place.

In the case of a sulphur-free buffer, general corrosion of the copper container can be determined by a simple calculation. The experimentally derived diffusion coefficient of aqueous sulphide in bentonite is approximately 7×10^{-8} cm²/s (King & Stroes-Gascoyne, 1995; King et al., 2002). The groundwater of the envisaged repositories in Finland, Sweden and Canada has sulphide concentrations in the range from $<3 \times 10^{-7}$ to 3×10^{-5} mol/L. Assuming sulphide concentrations at the upper limit, 6×10^{-17} mol/(s cm²) are transported through the 35 cm thick bentonite to the container surface. This is equivalent to a general corrosion rate of 3×10^{-8} cm/a, when Cu° is transformed to Cu_2S. Allowing for localised corrosion by multiplying the general rate with a correction factor of 5, the maximum corrosion depth is less than 0.2 cm within one million years. A service time for the 5-cm thick copper shell beyond one million years is a realistic possibility (Schwartz, 2008). The mass-transport assumption in this case sets an upper corrosion limit because some of the diffusing sulphide reacts with disseminated native-copper in the buffer and, therefore, is not available for corrosion of the copper container. Thus the near-field release for a canister that has no production defect and has not suffered mechanical damage is assumed to be zero for the 200,000-year simulation period.

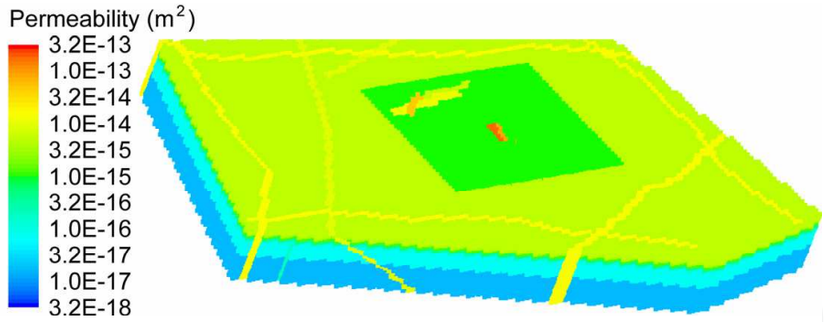

Fig. 14. Olkiluoto model. Block diagram

C	unlimited
Cl	unlimited
Cs	unlimited
I	unlimited
Ni	4.3×10^{-3}

Table 5. Olkiluoto model. Liquid-phase solubility (mol/L) in the near-field

4.3 Geometry of the far-field model and initialisation

The model has a total of 323,657 elements. The irregular rectangular primary mesh is the fracture continuum, which measures 7,700 m x 5,500 m x 750 m (Figs. 14-16) and consists of 27 layers with 168,048 cubic or cuboid cells. The nodal distance in the x and y direction is 66.6 m. The top layer has nodal z values representing the head (-8 m to 10 m altitude). The second layer has nodes located 0.1 m vertically below those of the top layer. The vertical nodal distance between the following 25 layers is 30 m. The top layer, which serves to maintain constant temperature, pressure and salinity, exclusively consists of infinite-volume boundary elements (10^{45} m^3). The bottom layer cells have a volume of 10^{14} m^3. This volume is large enough for maintaining nearly constant temperature and salinity throughout the simulation period but is simultaneously flexible enough to account for pressure adjustments. The volume of the remaining cells is calculated according to their nodal positions. The secondary matrix continuum comprises the layers 2 to 26. The detailed geometric relationships between fracture and matrix continuum are determined on the basis of a parameter estimation procedure (see "Parameter estimation").

The infinite-volume elements of the top layer have a pressure of 10^5 Pa, a temperature of 6°C and zero salinity. The bottom-layer large-volume elements (10^{14} m^3) have an initial temperature of 14°C and an initial salinity of 0.025 mass fraction salt (corresponding to 0.44 mol/L Cl). The remaining layers have initial values along the gradients defined by the top and bottom layers. These boundary conditions and initial conditions, together with a high diffusivity of salt (10^{-3} m^2/s), allow to maintain suitable vertical gradients throughout the simulation, unless disturbed by radioactive heat sources. These gradients include temperature and salinity gradients that are close to the present-day values (Pitkänen et al., 2004; Löfman, 2005).

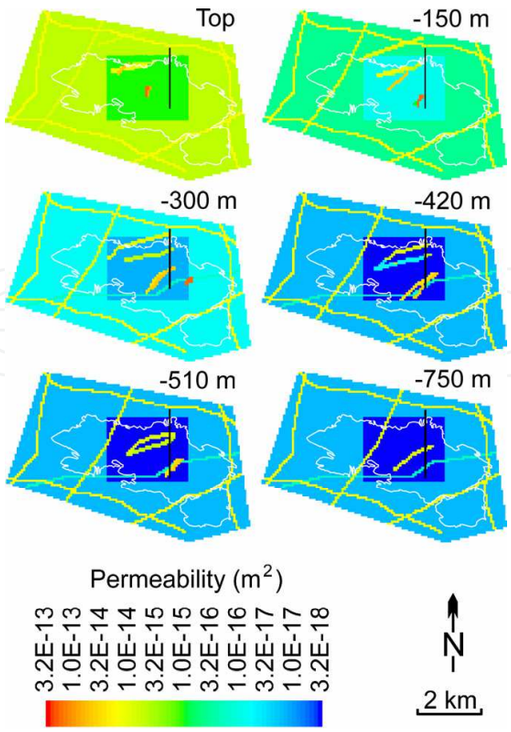

Fig. 15. Olkiluoto model. Permeability (m²) of the top, -150 m, -300 m, -420 m, -510 m and -750 m layer. The position of the parameter-estimation model (black solid line orientated N-S) is also shown

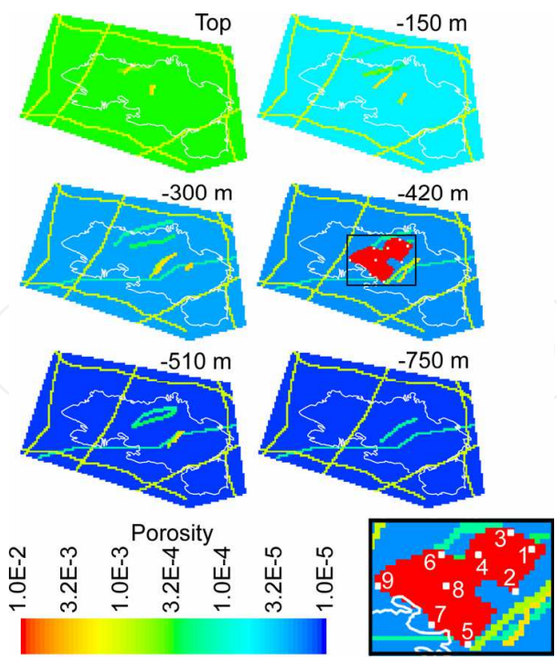

Fig. 16. Olkiluoto model. Flow porosity of the top, -150 m -300 m, -420 m, -510 m and -750 m layer. The repository area at the -420 m level is the red-coloured zone (indicating 0.01 porosity). Inset: The location of the source elements (1-9) in the repository area at the -420 m level

General properties				
Model length/width/height (m)	7,700/5,500/750			
Simulation period (a)	200,000			
Rock grain density (kg/dm^3)	2.7			
Rock grain specific heat (J/kg°C)	800			
Formation heat conductivity (W/m°C)	3.65			
Matrix porosity for anions (-)	0.001			
Matrix porosity for neutral species and cations (-)	0.005			
Flow porosity [average/range] (-)	6.6x10^{-5}/10^{-5}-10^{-3}			
Fracture spacing (m)	5			
Inventory				
C-14 (Bq/t U)	2.78x10^{10}			
Cl-36 (Bq/t U)	1.04x10^{9}			
Cs-135 (Bq/t U)	2.15x10^{10}			
I-129 (Bq/t U)	1.14x10^{9}			
Ni-59 (Bq/t U)	1.32x10^{11}			
	Distance factor (-)		**Retardation factor for the fracture continuum (-)**	
	15-continua models	**Dual-continuum models**	**15-continua models**	**Dual-continuum models**
C-14	1	0.04	1	1
Cl-36	1	0.45	1	1
Cs-135	1	0.022	1	50
I-129	1	0.46	1	1
Ni-59	1	0.019	1	70
	Distribution coefficient (dm^3/kg)		**Effective diffusivity (m^2/s)**	
C-14	0		1.0 x 10^{-13}	
Cl-36	0		1.0 x 10^{-14}	
Cs-135	50		1.0 x 10^{-13}	
I-129	0		1.0 x 10^{-14}	
Ni-59	100		1.0 x 10^{-13}	

Table 6. Set-up of the Olkiluoto model

The simulation period is 200,000 years. During the first 10,000 years, the terrain is subjected to glacio-isostatic uplift (POSIVA, 2006; Löfman & Poteri, 2008) and the transient head conditions are translated into transient mesh geometries. The head reference point, which is the vertical projection of the north-western corner of the repository, is fixed at a constant value (2 m). The z values of the top layer change from simulation year zero to year 1,000 and 10,000 according to the z values in Figure 17. The rising terrain implies a retreating shoreline of the Baltic Sea, indicated by the <0-m head contours moving away from the present island of Olkiluoto.

There are nine contaminant-injection cells evenly distributed over the repository area on the -420 m level (Fig. 16). These source cells have only one connection to a fracture element. The near-field releases of the radionuclides shown in Figure 12 are used as input (see "Near field"). Transport paths and, hence, travel times for the radionuclides strongly depend on the location within the repository from which they are released. An ideal simulation would include all repository cells but this is too expensive computationally. Scoping calculations indicate that the relevant results such as median, mean and maximum doses change little when more than nine source cells are used.

4.4 Hydraulic properties

The geometry of the Hydrogeological Zones (HZs) of high permeability and surrounding Sparsely Fractured Rock (SFR) of low permeability corresponds to the hydrogeological structure model of Vaittinen et al. (2009). Permeability and flow porosity (Figs. 15 and 16) are based on POSIVA (2009). The only exception is the repository area on the -420 m level, where the permeability is based on Vaittinen et al. (2009) and POSIVA (2009) but the flow porosity is 0.01; this flow porosity value is derived from a backfilled repository volume of 1,310,000 m^3 (Kirkkomäki, 2007) and an average backfill porosity of 0.35.

4.5 Heat sources

The heat production of the radioactive waste in a single canister is shown for the first 2,000 years after deposition in Figure 18. These values are multiplied by a factor of 8.8, which is the number of canisters in a model cell, and are used as heat-generation data for the repository area on the -420 m level.

4.6 Parameter estimation

The retention of radionuclides in a fractured medium is caused by diffusion from the fracture into the stagnant fluid of the matrix adjacent to the fracture. An ideal simulation of a fracture media problem would require the discretisation of the matrix continuum (multiple-interacting continua or MINC model; Pruess, 1983; Pruess & Narasimhan, 1985; Pruess, 1992; Xu & Pruess, 2001; Liou, 2007).

Ten or more matrix continua are necessary for accurately simulating diffusive transport between fracture and matrix as the comparisons between numerical and analytical solutions have shown (Tang et al., 1981; Sudicky & Frind, 1982; Wu & Pruess, 2000; Diersch, 2009). However, the resulting problem size would be too large in the case of a three-dimensional simulation. Therefore, the problem size has to be reduced by replacing

the model with a finely discretised matrix by an equivalent dual-continuum model (one matrix continuum). This is achieved by parameterising two variables among the three variables that control the retention of radionuclides; these are the diffusive transport distance between fracture and matrix, fluid volume of the fracture and effective diffusivity. The equivalent model is designed as conventional double-porosity model (Hantush et al., 2000, 2002; Lichtner, 2000).

The critical step in designing the model with a single matrix continuum (equivalent dual-continuum model) is the estimation of the parameters that justify to replace the corresponding finely discretised model (with a multi-continua matrix). The MINC pre-processor program of the TOUGHREACT code (Pruess et al., 1999) is suitable for models with up to 34 matrix continua. Scoping calculations have shown that models with 14 matrix continua have nearly the same retention properties as those of a model with the maximum number of continua. Thus, a two-dimensional 15-continua model has been designed that contains the fracture continuum of a 2,000-m long vertical subsection of the three-dimensional model enclosing the radioactive source element 1 (Figs. 15 and 16). A row of 14 matrix elements is connected to each fracture element with the exception of the fracture elements of the top and bottom layers.

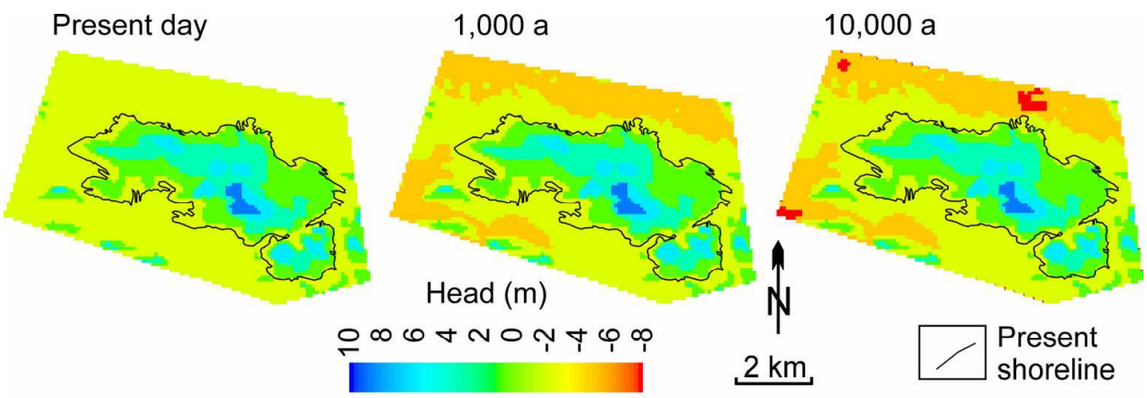

Fig. 17. Olkiluoto model. Vertical nodal positions (z coordinates; m) of the top layer in the simulation year zero, 1,000 and 10,000

The detailed geometry of the MINC mesh is calculated with the ONE-D proximity function of the MINC pre-processor program of the TOUGHREACT code. The fracture spacing is set at 5.0 m, which is the reciprocal of the weighted mean of the fracture intensity (Nykyri et al., 2008). The element volume fraction of the matrix continuum is derived from a matrix porosity of 0.001 for anions (Cl-36 and I-129) and 0.005 for neutral species and cations (C-14, Cs-135 and Ni-59) (Nykyri et al., 2008). According to the anion exclusion concept, anions and cations do not occupy the same pore system in low-porosity rocks, due to electrical forces caused by the usually negative charge of the mineral surfaces. Anions experience repulsion close to the mineral surfaces whereas cations are adsorbed on the surfaces (Rasilainen, 1997).

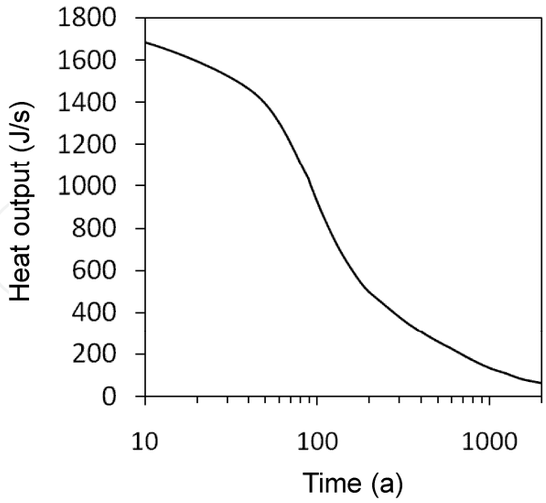

Fig. 18. Olkiluoto model. Heat output (J/s) from a canister with 1.93 t U burnt fuel from year 10 to year 2,000 after disposal (Löfman, 2005)

The near-field releases of radionuclides (Fig. 12) are used as input. The decay, diffusion and sorption data for the radionuclides (Tables 4 and 6; Nykyri et al., 2008) are the same as those for the three-dimensional far-field model.

Sorption of radionuclides takes place in the matrix continuum of the 15-continua model but not in the fracture continuum. The retardation factor $R_{m,i}$ of the radionuclide i (dimensionless) for the matrix continuum is calculated according to the equation

$$R_{m,i}=1+((1- n_m)K_{d,i}d)/n_m, \quad (4)$$

where n_m is the matrix porosity (dimensionless), d is the rock density (kg/dm^3) and $K_{d,i}$ is the distribution coefficient (dm^3/kg) of the radionuclide i for the rock matrix (Table 6).

TOUGHREACT calculates diffusion according to Fick's first law. The retention of radionuclides is controlled by the diffusivity, the fluid volume and transport distance between fracture and matrix. A dual-continuum model can almost perfectly substitute the 15-continua model if only two variables are parameterised; e.g., the fluid volume of the fracture together with the transport distance between fracture and matrix (as applied here) or the fluid volume of the fracture together with the diffusivity (producing similar results).

The fluid volume of the fracture continuum is adjusted by parameterising the retardation factor of the fracture continuum (which equals unity in the 15-continua model). The diffusive transport distance is parameterised by multiplying the fracture spacing of the 15-continua model (5 m) with a distance factor. The parameters are determined by the log-least-squares method. This method minimises the squared deviations between the annual far-field releases of the dual-continuum model and those of the 15-continua model (Fig. 19; Table 6). Note that the annual far-field release of a radionuclide (Bq/a) is the annual transport of the radionuclide from the second topmost layer to the topmost layer of the two-dimensional model.

The parameters obtained from this optimised two-dimensional model are used for the three-dimensional model that has one fracture continuum and one matrix continuum. This equivalent dual-continuum model is used for the subsequent transport simulations.

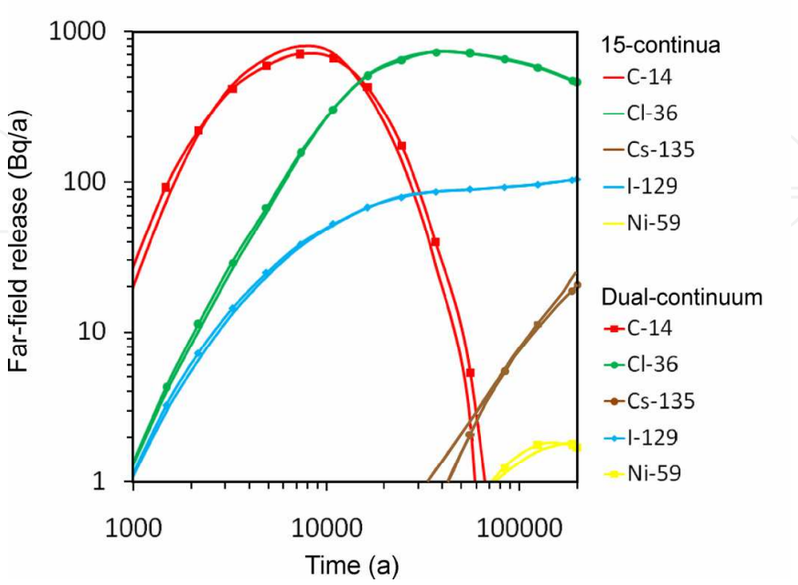

Fig. 19. Parameter estimation for the Olkiluoto model. The far-field release of radionuclides is shown for a 15-continua model and the equivalent dual-continuum model (optimised model)

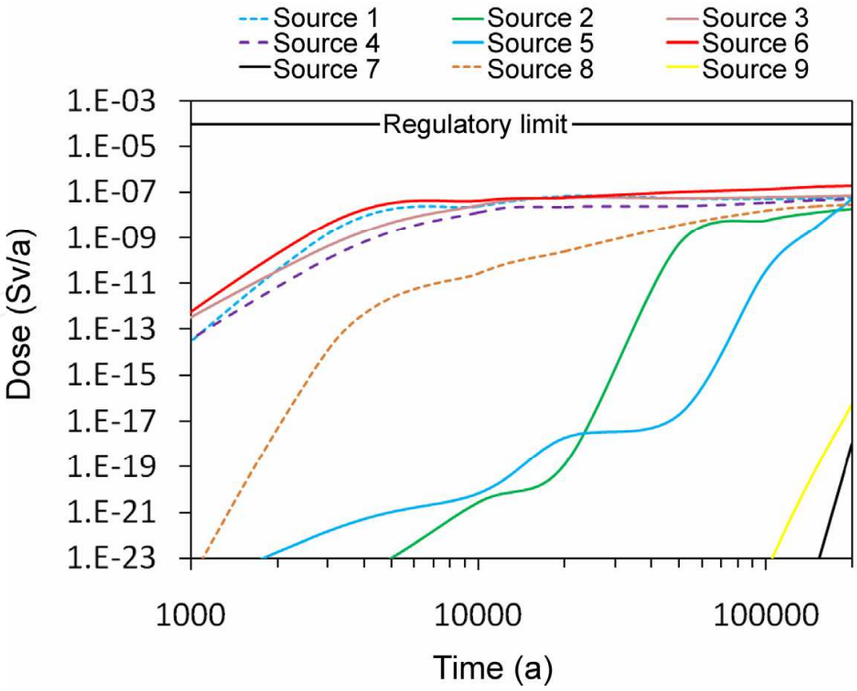

Fig. 20. Olkiluoto model. Peak values of the radioactive dose (Sv/a) for the second topmost layer for the sources 1-9

4.7 Simulated far-field transport

The radionuclide releases of the near-field base case are used as input for the far-field simulations. The biosphere is represented by the second topmost layer of the far-field model, which has fresh-water quality for most of the simulation period. The near-field base case assumes that one canister randomly chosen in the repository layout has a defect. There is a strong variability of radioactivity released to the biosphere depending on the location of the defective canister (Fig. 20). The canister locations 1-4, 6 and 8 in the north-eastern and central part of the repository imply a relatively large amount of radioactivity released to the biosphere whereas canisters located at the positions 5, 7 and 9 in the south-western part imply low or insignificant amounts of radioactivity. Figures 21A and 21B show the contaminant plumes for the source 3 at the NE corner and source 5 at the SE corner of the repository, respectively. The plumes emanating from the remainder of the canister locations have shapes that are intermediate between those shown. The maximum dose, which is produced by the canister position 6 (1.2×10^{-7} Sv/a), is far below the Finish regulatory limit of 1×10^{-4} Sv/a.

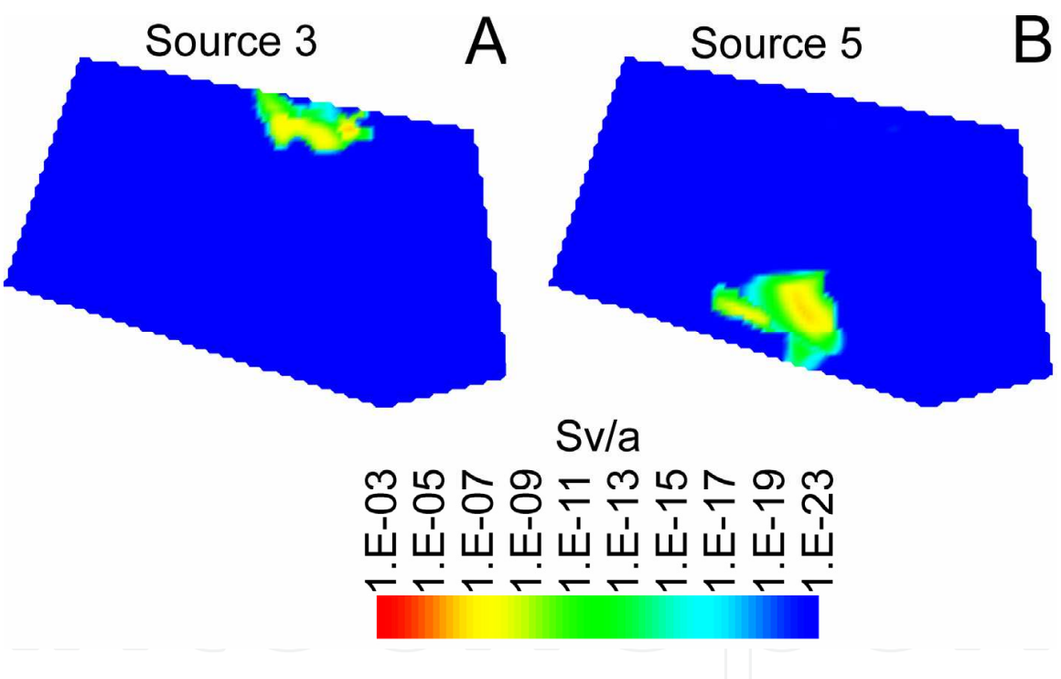

Fig. 21. Olkiluoto model. (A and B) Maps of the second topmost layer with radioactive dose (Sv/a) in the simulation year 200,000 for the sources 3 and 5

5. The Opalinus-Clay repository

The current scenarios assume that the repository will be located in the Jurassic Opalinus Clay in the Zürcher Weinland region, Switzerland (Fig. 1; NAGRA 2002). The claystone formation is gently dipping and has a thickness of 105-125 m. It is overlain by Middle Jurassic through Pleistocene sediments of approximately 600 m thickness. About 2,800 waste

canisters containing 3,200 t U burnt fuel will be deposited in near-horizontal emplacement tunnels, which are connected to an access ramp via operational tunnels.

Two types of waste containers are considered for the repository. The first option is a steel canister, which is similar to that envisaged for the Gorleben repository. The second option is a container with a corrosion-resistant copper shell, such as the canisters for the Olkiluoto repository. So far, only the near-field release for the first option has been published (NAGRA, 2002; Kosakowski, 2004). For the second option, which considers improved safety standards, there are no near-field data available. The hydrochemical regime of a clay repository is similar to that of a granitoid repository but totally different from the highly corrosive regime of a salt repository. The performance of a copper-cast iron canister in a clay repository is as good as the performance of such a canister in a granitoid repository. Except for the case of a production defect or mechanical damage, the canister can assumed to be isolating the waste for a period of more than one million years. The permeability of a clay host rock is less than the permeability of a granitoid host rock. Thus it can be assumed that the potential groundwater contamination caused by a defective canister in the Opalinus-Clay repository is not higher than that for the Olkiluoto granitoid repository if the same type of waste canister is used.

6. Conclusions

The quality of models for groundwater contamination above high-level repositories in granitoid, salt and clay is not uniform. The most problematic case is a salt repository for two main reasons. First, the plastic behaviour of the host rock (salt) is a variable that introduces a high degree of uncertainty in any model attempt. Second, there is the inevitable generation of hydrogen gas caused by the corrosion of the steel waste canisters in high-salinity environments at low oxygen fugacities. The conditions of gas release constitute a great source of uncertainty. There is the possibility of unsteady or explosive release of hydrogen gas transporting short-lived radionuclides (Schulze, 2002). Furthermore, the permeability of the backfill of the shaft, through which the gas is assumed to flow, has a strong influence on the performance of the repository.

For a steady (non-explosive) gas release, a backfill permeability of $\leq 10^{-12}$ m^2 results in a radioactive dose of about 1 mSv/a. A higher permeability would decrease the radioactive dose to values below the German regulatory limit (0.1 mSv/a). A relatively high permeability favours the flow of liquid with respect to the flow of gas whereas a relatively low permeability has the opposite effect. A low permeability is the appropriate safety concept for a one-phase scenario (only liquid); however, a high permeability is the appropriate concept for a two-phase scenario (liquid and gas). As both scenarios are equally realistic, there is a typical conflict of targets. Such problems are not an important issue for the standard concept of a granitoid-hosted repository and the non-standard concept of a clay-hosted repository (both with copper-cast iron waste containers).

7. References

Beushausen, M. & Ludwig, R. (1990). Hydrogeologische Gliederung der oberoligozänen und miozänen Schichten. Bundesanstalt für Geowissenschaften und Rohstoffe, Hannover, Germany, Report Archive No. 106036, various paginations.

Brooks, R.H. & Corey, A.T. (1964). Hydraulic properties of porous media. *Hydrology Papers Colorado State University Fort Collins*, Vol. 3, pp. 1-27.

Corey, A.T. (November 1954). The interrelation between gas and oil relative permeabilities. *Producer's Monthly*, Vol. 19, No. 1 (quoted by Brooks and Corey 1964).

Diersch, H.J. (2009). *FEFLOW reference manual*. DHI-WASY GmbH, Berlin, Germany. URL: www.feflow.info/manuals.html

Hantush, M.M., Mariño, M.A. & Islam, M.R. (2000). Models for leaching of pesticides in soils and groundwater. *Journal of Hydrology*, Vol. 227, pp. 66-83.

Hantush, M.M., Govindaraju, R.S., Mariño, M.A. & Zhang, Z. (2002). Screening model for volatile pollutants in dual porosity soils. *Journal of Hydrology*, Vol. 260, pp. 58-74.

Hirsekorn, R.P., Nies, A., Rausch, H. & Storck, R. (1991). Performance assessment of confinements for medium-level and a-contaminated waste (PACOMA Project). GSF report 12/9 (GSF-Forschungszentrum für Umwelt und Gesundheit, Braunschweig, Germany), various paginations.

Javeri, V. (2006). Three-dimensional analyses of coupled gas, heat and nuclide transport in a repository including rock salt convergence. *Proceedings of the TOUGH Symposium 2006, 15-17 May 2006*, pp. 1-9, Lawrence Berkeley National Laboratory, Berkeley, California, U.S.A.. URL: http://esd.lbl

Keesmann, S., Nosek, U., Buhrmann, D., Fein, E. & Schneider, A. (2005). Modellrechnungen zur Langzeitsicherheit von Endlagern in Salz- und Granit-Formationen. GRS - Gesellschaft für Anlagen- und Reaktorsicherheit, Braunschweig, Germany, Report GRS-206, various paginations.

King, F. & Stroes-Gascoyne, S. (1995). Microbially influenced corrosion of nuclear fuel waste disposal containers. *Proceedings. Int. Conf. on Microbially Influenced Corrosion*, NACE International and American Welding Society, pp. 35/1-35/14.

King, F., Ahonen, L., Taxen, C., Vuorinen, U. & Werme, L. (2002). Copper corrosion under expected conditions in a deep geologic repository. *POSIVA Report* 2002-01. ULR: www.posiva.fi

Kirkkomäki, T. (2007). Design and stepwise implementation of the final repository (in Finnish, English abstract). *POSIVA Työraportty* 2006-92. URL: www.posiva.fi

Klinge, H., Boehme, J., Grissemann, C., Houben, G., Ludwig, R., Rübel, A., Schelkes, K., Schildknecht, F. & Suckow, A. (2007). Standortbeschreibung Gorleben Teil 1: Die Hydrogeologie des Deckgebirges des Salzstocks Gorleben. *Geologisches Jahrbuch*, Vol. C71, pp. 5-147.

Klinge, H., Margane, A., Mrugalla, S., Schelkes, K. & Söfner, B. (2001). Hydrogeologie des Untersuchungsgebietes Dömitz-Lenzen. Bundesanstalt für Geowissenschaften und Rohstoffe, Hannover, Germany, Report Archive No. 0121207, various paginations.

Kosakowski, G. (2004). Time-dependent flow and transport calculations for project Opalinus Clay (Entsorgungsnachweis). *NAGRA Technical Report* 03-10. URL: www.nagra.ch

Lichtner, P.C. (2000). Critique of dual continuum formulations of multicomponent reactive transport in fractured porous media. *Los Alamos National Laboratory Report* LA-UR-00-1097. URL: www.osti.gov

Liou, T.S. (2007). Numerical analysis of a short-term tracer experiment in fractured sandstone. *Terrestrial Atmospheric Oceanic Sciences*, Vol. 18, pp. 1029-1050.

Löfman, J. (2005). Simulation of hydraulic disturbances caused by the decay heat of the repository in Olkiluoto. *POSIVA Report* 2005-07. URL: www.posiva.fi

Löfman, J. & Poteri, A. (2008). Groundwater flow and transport simulations in support of RNT-2008 analysis. *POSIVA Working Report* 2008-52. URL: www.posiva.fi

Ludwig, R., Mandl, J. & Uhlig, A. (1989). Zwischenbericht über die Diskretisierung hydrogeologischer Strukturen im Bereich Gorleben. Bundesanstalt für Geowissenschaften und Rohstoffe, Hannover, Germany, Report Archive No. 0105061, various paginations.

Ludwig, R., Schneider, M. & Sewing, D. (1993). Projekt Gorleben: Hydrogeologische Gliederung der quartärzeitlichen Schichtenfolge. Bundesanstalt für Geowissenschaften und Rohstoffe, Hannover, Germany, Report Archive No. 110256, various paginations.

NAGRA (2002). Project Opalinus Clay - safety report. *NAGRA Technical Report* 02-05. URL: www.nagra.ch

Nykyri, M., Nordman, H., Marcos, N., Löfman, J., Poteri, A. & Hautojärvi, A. (2008). Radionuclide release and transport - RNT-2008. *POSIVA Report* 2008-06. URL: www.posiva.fi

Pitkänen, P., Partamies, S. & Luukkonen, A. (2004). Hydrochemical interpretation of baseline groundwater conditions at the Olkiluoto site. *POSIVA Report* 2003-07. URL: www.posiva.fi

POSIVA (2006). Expected evolution of a spent nuclear fuel repository at Olkiluoto. *POSIVA Report* 2006-05. URL: www.posiva.fi

POSIVA (2009). Olkiluoto site description 2008. *POSIVA Report* 2009-1. URL: www.posiva.fi

Prikryl, R. & Woller, F. (April 2002). Going underground – a new market for Czech bentonite in nuclear waste disposal. *Industrial Minerals*, pp. 72-77.

Pruess, K. (1983). GMINC - a mesh generator for flow simulations in fractured reservoirs. *Lawrence Berkeley National Laboratory Report* LBL-15227. URL: http://esd.lbl

Pruess, K. & Narasimhan, T.N. (February 1985). A practical method for modeling fluid and heat flow in fractured porous media. *Society Petroleum Engineers Journal*, pp. 14-26.

Pruess, K. (1992). Brief guide to the MINC-method for modeling flow and transport in fractured media. *Lawrence Berkeley National Laboratory Report* LBL-32195. URL: http://esd.lbl

Pruess, K., Oldenburg, C. & Moridis, G. (1999). TOUGH2 user's guide, version 2.0. *Earth Sciences Division, Lawrence Berkeley National Laboratory, University of California*, Berkeley, U.S.A.. URL: http://esd.lbl

Rasilainen, K. (1997). Matrix diffusion model. *VTT Publication* 331 (ESPOO, Helsinki, Finland). www.vtt.fi/inf/pdf/publications/1997/P331.pdf

Rasmussen, T.C. (2001). Pressure wave vs. tracer velocities through unsaturated fractured rock. *American Geophysical Union Geophysical Monograph*, Vol. 42, pp. 45-52.

Schulze, O. (2002). Auswirkung der Gasentwicklung auf die Integrität geringdurchlässiger Barrieregesteine. Bundesanstalt für Geowissenschaften und Rohstoffe, Hannover, Germany, Report Archive No. 0122442, 142 pp.

Schwartz, M.O. (1996). Native copper deposits and the disposal of high-level waste. *International Geology Review*, Vol. 38, pp. 33-41.

Schwartz, M.O. (2008). High-level waste disposal, ethics and thermodynamics. *Environmental Geology*, Vol. 54, pp. 1485-1488.

SKB (2006). Long-term safety for KBS-3 repositories at Forsmark and Laxemar - a first evaluation. *SKB Technical Report* TR-06-09. URL: www.skb.se

SKI (2006). Engineered barrier system - assessment of the corrosion properties of copper canisters. *SKI Report* 2006:11. URL: www/ski.se

Storck, R., Aschenbach, J., Hirsekorn, R.P., Nies, A. & Stelte, N. (1988). PAGIS performance assessment of geological isolation systems for radioactive waste: disposal in salt formations. *Office for Official Publications of the European Communities*, Luxembourg.

Sudicky, E.A. & Frind, E.O. (1982). Contaminant transport in fractured porous media: Analytical solutions for a system of parallel fractures. *Water Resources Research*, Vol. 18, pp. 1634-1642.

Suter, D., Biehler, D., Blasser, P. & Hollmann, A. (1998). Derivation of a sorption data set for the Gorleben overburden. *Proceedings DisTec'98, September 9-11, 1998*, pp. 581-584, Hamburg, Germany.

Tang, D.H., Frind, E.O. & Sudicky, E.A. (1981). Contaminant transport in fractured porous media: Analytical solution for a single fracture. *Water Resources Research*, Vol. 17, pp. 555-564.

Vaittinen, T., Ahokas, H. & Nummela, J. (2009) Hydrogeological structure model of the Olkiluoto site - update in 2008. *POSIVA Working Report* 2009-15. URL: www.posiva.fi

Van Genuchten, M.T. (1980). A closed-form equation for predicting the hydraulic conductivity of unsaturated soils. *Soil Science Society America Journal*, Vol. 44, pp. 892-898.

Vogel, P. (2005). Orientierende 3-D-Grundwassermodellrechnungen auf den Strukturen eines hydrogeologischen Modells Gorleben. Bundesanstalt für Geowissenschaften und Rohstoffe, Hannover, Germany, Report Archive No. 0125865, 70 pp.

Wu, Y.S. & Pruess, K. (2000). Numerical simulation of non-isothermal multiphase tracer transport in heterogeneous fractured porous media. *Advances in Water Resources*, Vol. 23, pp. 699-723.

Xiao, Z., Gammons, C.H. & Williams-Jones, A.E. (1998). Experimental study of copper(I) chloride complexing in hydrothermal solutions at 40 to 300°C and saturated vapor pressure. *Geochimica et Cosmochimica Acta*, Vol. 62, pp. 2949-2964.

Xu, T. & Pruess, K. (2001). Modeling multiphase non-isothermal fluid flow and reactive geochemical transport in variably saturated fractured rocks: 1. Methodology. *American Journal Science*, Vol. 301, pp. 16-33.

Xu, T., Sonnenthal, E., Spycher, N. & Pruess, K. (2005). TOUGHREACT user's guide: a simulation program for non-isothermal multiphase reactive geochemical transport in variably saturated geologic media. *Earth Sciences Division, Lawrence Berkeley National Laboratory, University of California*, Berkeley, U.S.A.. URL: http://esd.lbl

Zhang, K., Wu, Y. & Pruess, K. (2008). User's guide for TOUGH2-MP - a massively parallel version of the TOUGH2 code. *Earth Sciences Division, Lawrence Berkeley National Laboratory, University of California*, Berkeley, U.S.A.. URL: http://esd.lbl

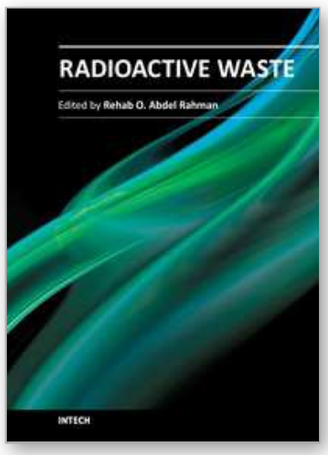

Radioactive Waste

Edited by Dr. Rehab Abdel Rahman

ISBN 978-953-51-0551-0
Hard cover, 502 pages
Publisher InTech
Published online 25, April, 2012
Published in print edition April, 2012

The safe management of nuclear and radioactive wastes is a subject that has recently received considerable recognition due to the huge volume of accumulative wastes and the increased public awareness of the hazards of these wastes. This book aims to cover the practice and research efforts that are currently conducted to deal with the technical difficulties in different radioactive waste management activities and to introduce to the non-technical factors that can affect the management practice. The collective contribution of esteem international experts has covered the science and technology of different management activities. The authors have introduced to the management system, illustrate how old management practices and radioactive accident can affect the environment and summarize the knowledge gained from current management practice and results of research efforts for using some innovative technologies in both pre-disposal and disposal activities.

InTech Europe
University Campus STeP Ri
Slavka Krautzeka 83/A
51000 Rijeka, Croatia
Phone: +385 (51) 770 447
Fax: +385 (51) 686 166
www.intechopen.com

InTech China
Unit 405, Office Block, Hotel Equatorial Shanghai
No.65, Yan An Road (West), Shanghai, 200040, China
中国上海市延安西路65号上海国际贵都大饭店办公楼405单元
Phone: +86-21-62489820
Fax: +86-21-62489821

IntechOpen